Annealing Steel Coils

Mark McGuinness, Victoria University of Wellington, New Zealand
Winston L. Sweatman, Massey University, Auckland, New Zealand
Duangkamon (Yui) Baowan, University of Wollongong, Australia
Steve I. Barry, UNSW@ADFA, Canberra, ACT, Australia.

Abstract

Cold rolled steel in the form of coiled sheet requires heat treatment (annealing) in order to release stresses and reform the crystalline structure. During this process the whole coil must be heated to the required temperature and then maintained at this temperature for a period of time. At New Zealand Steel the process takes place inside a batch annealing furnace. The MISG group considered the problem of where the cold point lies within the steel coils, i.e. what is the last part of the coil to reach the required temperature, and how long does it take to reach this temperature? Challenges include deciding what the boundary conditions are on a coil, and dealing with the nonlinearity and anisotropy caused by expanding gaps within coils.

1 Introduction

During steel manufacture, the process of cold rolling introduces stresses due to changes in the crystalline structure of the metal. These stresses are released by further heat treatment (annealing) which reforms the crystalline structure and reintroduces desirable mechanical properties. The steel for this stage is in the form of a coil. The coil has been produced by wrapping a long steel sheet about an armature, which is then removed, leaving a curved inner surface. The entire steel coil has to be raised to a specified temperature within a *Uniflow Annealing System* (UAS) furnace. The steel coil is then maintained at this temperature for a period of time to achieve annealing.

New Zealand Steel have a number of formulae that they use to decide how long to keep a set of coils in the furnace, to ensure the thermal centre of each

coil reaches the desired temperature. These formulae were derived from data generated during commissioning of the furnace, and subsequently lost. The formulae have also been modified over the years, and the original formulae are no longer available. The industry representatives asked MISG to use mathematical modelling to decide

1. Do the existing heating equations accurately predict heating times based on coil weight and width?

2. Do we need to factor strip thickness into the heating equations?

To answer these questions, we need to model the heat transfer from the furnace through the steel coils. It is desired to determine the internal point within each coil that takes the longest time to reach the required temperature, and to find how much time is necessary for that to occur. Two parts to the problem were identified. One was to establish the boundary conditions at the exterior of the steel coils and the other was to model the internal conduction within the steel coils. In both these areas information and insight were provided by the industry representatives and from the literature.

2 Conditions within the UAS furnace

For the New Zealand Steel annealing process, batches of steel coils are placed upon a ventilated steel platform in a single layer on their circular ends (see Fig. (1)). The ventilation consists of vertical holes completely through the platform. Typically there are nine coils in a square formation on the platform. Each coil weighs between ten and twenty tonnes, is 700 to 1500mm high (this is the width of the steel strip before being coiled), and the steel strips are from 0.4 to 3mm thick.

The ventilated platform is transported through the front door of the furnace to initiate the heating process. After annealing is complete the platform exits at the back of the furnace into another chamber. The furnace is filled with heated gas, an inert mixture of nitrogen (93% by volume) and hydrogen. This is circulated around the coils. Heating is by radiant burners in the ceiling and sides of the furnace. The burners at the sides are shrouded so that they

do not radiatively heat the coils, but they do heat the gas. The burners in the ceiling are almost uniformly spread over the set of nine coils.

Figure 1: Photographs of steel coils being prepared for and entering the UAS furnace.

It is difficult to determine exact boundary conditions for the steel coils. There is limited experimental data available and the gathering of such data is difficult. Temperature has been recorded at two points — one in contact with the top surface of one of the steel coils and the other directly above this position and within the heated gas — leading to data like that illustrated in Fig. (2). New Zealand Steel use several different empirical formulae for deciding upon the duration of annealing. These are based on experience and previous commissioning experiments, from which there are no surviving data. The fits to these data have been modified from time to time, and the original fits have been lost.

Considering an individual steel coil, heat transfer is achieved by a mixture of direct radiation from the heaters on the roof of the furnace, conduction from the ventilated steel platform below the coils, and convection by the inert

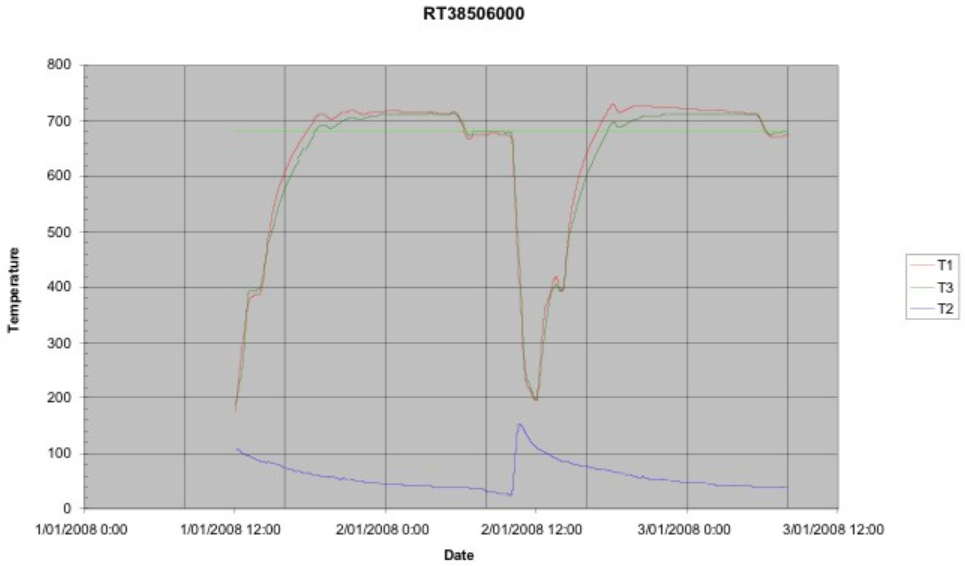

Figure 2: Temperature measurements (°C) taken in the hot gas above a set of coils, and in contact with the upper outer edge of a coil, inside a UAS furnace during one-and-a-bit heating cycles. The upper curve is the gas temperature, and the one just below it is the contact temperature. The straight line is the target temperature.

gas (nitrogen/hydrogen mixture) which is blown over heaters and around the coils inside the furnace. The measurements in Fig. (2) indicate that the temperature on the circular top of the coil is very close to that of the neighbouring gas. This is likely due to rapid direct radiative heating of the top of the coil by the heaters in the ceiling. As a consequence, the upper boundary is here assumed to have a temperature that matches the furnace gas temperature. The circular base of the coil is assigned this temperature too, as the ventilated steel platform with its relatively large surface area is anticipated to heat very rapidly to the gas temperature, and then conduct heat directly into the lower end of each coil. Heating on the curved inner and outer surfaces of a coil is by convection from the surrounding gas and so the boundary condition here is that of Newton's Law of Cooling.

3 Heat transport within the coils

Superficially, each steel coil can be considered to be a hollow cylinder, annular in cross-section. However, as the coils are rolls of sheets of steel, there are gaps in the radial direction between the neighbouring parts of the steel sheet. As the gas in these gaps has a lower conductivity than steel, the effective conductivity of the coil in the radial direction is lower than that in the vertical direction (within the steel sheet). As a first approximation, the gap between the sheets is assumed to be constant. However, in practice, due to the nonuniformity of the rolling process, the steel sheet has a crown, that is it is thicker in the middle of the sheet than at the edges. This means that the radial gap varies in width vertically along the coil, being larger at the top and bottom ends of the coil, and smaller halfway up, where it is primarily due to surface roughness that there is a gap present. In principle, the thermal conductivity in the radial direction also varies with coil tension and differential heat expansion of the coils due to temperature gradients, and is dependent on radial position as well as vertical position. When there is contact between the radial steel layers, heat transport could occur through steel-steel contact[4], by diffusion through the gas in the gap, and by radiation across the gap. However, to a reasonable extent, a rough contact surface can still be treated as if it were effectively a small uniform width gap [8, 7].

Hence since the number of windings in each one is large, we model a coil as

a uniform hollow cylinder with radial conductivity dependent on position:

$$\frac{\partial(c_p \rho T)}{\partial t} = \frac{1}{r}\frac{\partial}{\partial r}\left(k_r r \frac{\partial T}{\partial r}\right) + \frac{\partial}{\partial z}\left(k_z \frac{\partial T}{\partial z}\right) \tag{1}$$

where T [K] is the temperature, c_p [J/Kg/K] the heat capacity which is a function of temperature, ρ [kg/m^3] the density of the steel, $k_r(z)$ [J/m/s/K] the radial conductivity, k_z [J/m/s/K] the vertical conductivity which is assumed to be the constant conductivity of steel, k_s.

The relevant dimensions and properties are listed in Table (1).

steel density	ρ	7854	kg/m^3 (at 300k)
steel thermal conductivity	k_s	60.5	W/m/K at 300K
		56.7	W/m/K at 400K
		48	W/m/K at 600K
		39.2	W/m/K at 800K
		30	W/m/K at 1000K
steel thermal capacity	C_p	434	J/kg/K at 300K
		487	J/kg/K at 400K
		559	J/kg/K at 600K
		685	J/kg/K at 800K
		1169	J/kg/K at 1000K
gas thermal conductivity	k_g	0.06	W/m/K
furnace circulation		800	m^3/minute
steel strip thickness		0.4–3	mm
steel strip width		700–1500	mm
coil mass		10–20	tonnes
coil inner diameter		508	mm
coil outer diameter		1.5	m
platform mass		37	tonnes
furnace dimensions		6.5x6.5x4	m^3

Table 1: Table of steel and coil properties

3.1 Radial Conductivity — Modelling the Gaps

In some of the literature [5, 6], the coils are modelled as a concentric series of separate annular cylinders of metal with hot gas between, as illustrated in

Fig. (3). Then variations in these radial gaps due to crowning (varying strip thickness) and due to temperature gradients inducing differential expansions have been calculated [5, 6].

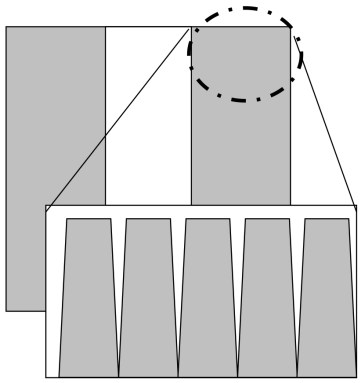

Figure 3: A sketch illustrating how variation in strip thickness causes a variation with height in the gas gap in the coils.

Using the geometry provided by New Zealand Steel, and sketched in Fig. (4), the effective radial thermal conductivity is

$$k_{\text{eff}} = \frac{a+b}{\frac{a}{k_s}+\frac{b}{k_g}} \ , \quad 550 \geq z \geq 419.74 \ ,$$

and in this z range,

$$a + b = d \ , \quad b = s(z - 418.42) \ ,$$

where measurements indicate that the slope s is 0.038/50. With a 1μm gap in the central contact region (an effective gap due to roughness),

$$k_{\text{eff}} = \frac{d}{1E-06/k_g + (d-1e-06)/k_s} \ , \quad z \leq 419.74 \ .$$

Using these equations, the effective radial thermal conductivity is in the range 14–25 W/m/K when d is in the range 0.4–3 mm. These thermal conductivities are plotted in Fig. (5). Note that these radial thermal conductivities are smaller than the vertical thermal conductivity, $k_s = 30$ W/m/K at 1000K.

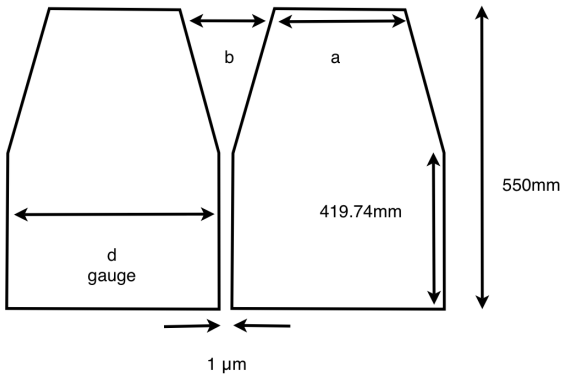

Figure 4: A sketch showing the geometry of the hot gas gap between two sheets of steel in a coil. The sketch shows the upper half of a cross-section through two 1.1m wide sheets.

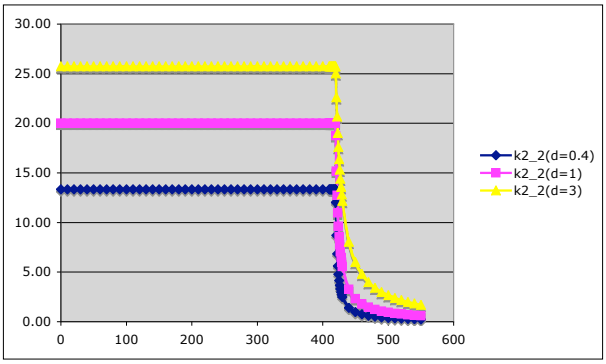

Figure 5: Effective radial thermal conductivities (W/m/K) resulting from the geometry sketched in Fig. (4), plotted against vertical distance from the middle of a coil (mm), for gauges $d = 0.4$, 1, and 3 mm, and for a temperature of 1000K.

3.2 Estimates of heating times

The timescale for heating is

$$t = \ell^2 \frac{\rho C_p}{k}$$

where ℓ is the lengthscale, and k is the appropriate (effective) thermal conductivity. This formula assumes that the surface of the steel is immediately raised to the target temperature.

So an approximate estimate of the time to heat a coil of steel, if there is only axial (vertical) heating, is

$$t = 10 - 50 \text{ hours} \tag{2}$$

for $\ell = 350$–750mm (half the height of a coil) and using $k = k_s$. A solution of the heat equation in the vertical direction with upper and lower surfaces fixed at T_{gas} obtained using Maple, is shown in Fig. (6).

And for purely radial heating, near the centre of the coil, so that $\ell = 250$mm, the heating times are

$$\begin{aligned} t &= 12 \text{ hrs}, \qquad \text{when } d = 0.4 \text{ mm} \\ t &= 8 \text{ hrs}, \qquad \text{when } d = 1 \text{ mm} \\ t &= 6 \text{ hrs}, \qquad \text{when } d = 3 \text{ mm} \end{aligned} \tag{3}$$

3.2.1 Radial Boundary Condition

However, radial heating is driven by conduction from the hot gas rather than by direct radiant heating from the furnace burners. Then the above heating times need to be reconsidered in light of the heat transfer coefficient H. The heat flux into the curved surfaces (inner and outer) of the coils when they are at temperature T is

$$Q_c = H(T_{\text{gas}} - T) \ ,$$

where

$$H = \frac{\text{Nu}\, k_g}{D}$$

and Nu is the Nusselt number (the ratio between actual — convective — heat transfer and that which would be achieved with only conductive processes at

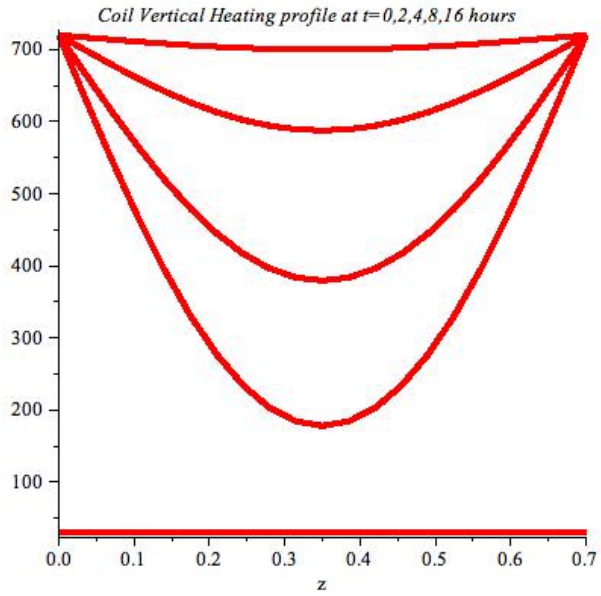

Figure 6: Solutions calculated by Maple to the axial (vertical) heating problem, using $k_s = 30$ W/m/K, $C_p = 1169$ J/kg/K, $T = 720$°C top and bottom, and initial temperature 30°C. Temperature (°C) is plotted against vertical distance (m) from the bottom of the steel coil. Time zero is the lowest curve; 16 hours of heating is the uppermost curve, in which the temperature in the coil is everywhere close to 720°C.

work in the hot gas), and D is the hydraulic diameter of the region the hot gas is flowing through. A number of semi-empirical formulae exist for Nu in the case of forced convection, in terms of the Reynolds number Re ($\approx 2.7\times10^4$ for the UAS furnace) and the Prandtl number Pr ≈ 0.7, including the laminar flow case:

$$\mathrm{Nu} = 0.648\sqrt{\mathrm{Re}}\,(\mathrm{Pr})^{\frac{1}{3}} \ ,$$

and in the turbulent flow case, the Dittus-Boelter formula

$$\mathrm{Nu} = 0.023\mathrm{Re}^{0.8}\mathrm{Pr}^{0.3}$$

and the Gnielinski formula

$$\mathrm{Nu} = \frac{0.037\mathrm{Re}^{0.8}}{1 + 2.443\mathrm{Re}^{-0.1}(\mathrm{Pr}^{2/3} - 1)}$$

All of these formulae give values for H in the range 3–5.

The question addressed here is whether the rate of heat transfer from the hot gas is the main limitation, or the rate at which heat is conducted radially into the steel coil from its surface. The Biot number helps answer this, since it is the ratio of the heat transfer rate at the surface to the heat transfer rate inside the coil:

$$\mathrm{Bi} = \frac{H\ell}{k_s} \approx 0.1 \ ,$$

and this value being much less than 1 says that the rate-limiting factor for radial heat transfer, is heat transfer from the hot gas to the surface of the coil, rather than within the coil. This calculation is supported by numerical solutions to the radial heat equation using Maple, illustrated in Fig. (7). In this figure, the internal temperatures stabilise much faster than the overall temperature rises.

This implies that the details of how the radial thermal conductivity vary with height and with temperature gradients are less important than heat transfer across a thermal boundary layer in the hot gas to the curved vertical surfaces of a coil, and that heat transfer in the vertical direction is much more rapid, despite the longer distances involved, because radiation and the plenum can transfer much more heat to the horizontal surfaces.

Furthermore, discussion with the industry representatives suggested that the tensions and roughness of the actual coils would tend to reduce the variations

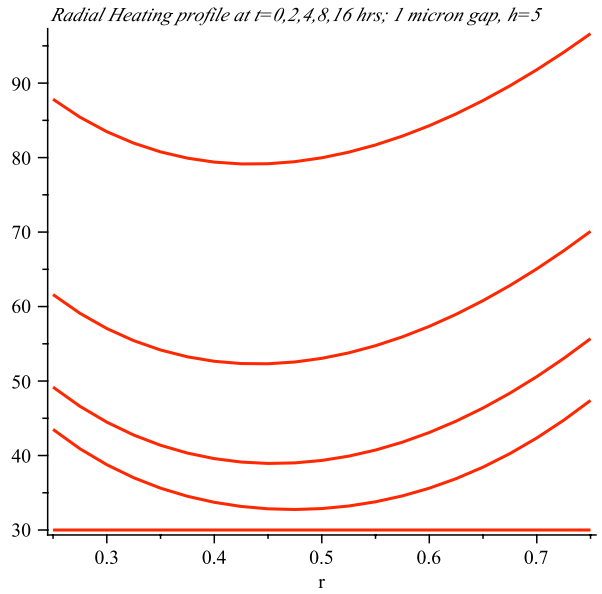

Figure 7: Solutions calculated by Maple to the radial heating problem, using $H = 5$ in the flux boundary condition, $k_s = 20$ W/m/K, $C_p = 1169$ J/kg/K, $T_{\text{gas}} = 720°\text{C}$, and initial temperature 30°C. Temperature (°C) is plotted against radial distance (m) from the centre of the annulus that is the cross-section of the steel coil. Time zero is the lowest curve; 16 hours of heating is the uppermost curve. Note the relatively slow rise in boundary temperatures. Also note that the coldest point is nearer the inner face of the coil, due to its smaller surface area (hence smaller heat flux).

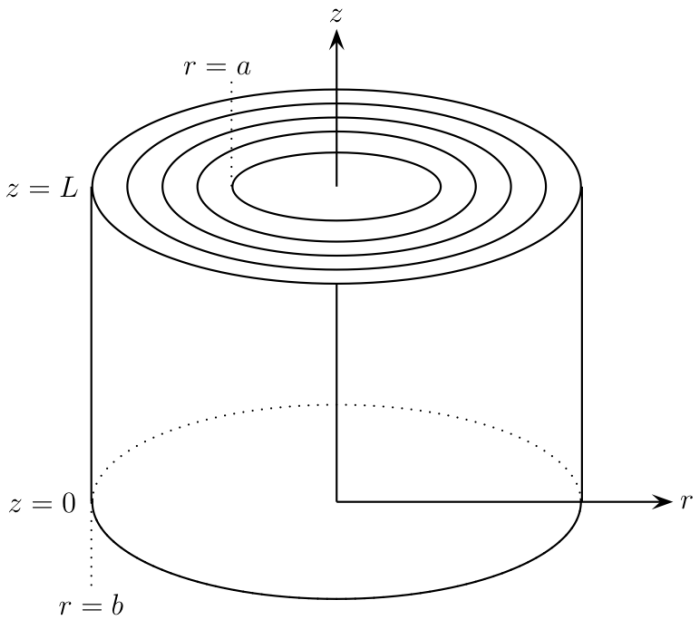

Figure 8: Schematic of nested cylinders of height $z = L$ and radius $r \in [a, b]$.

with height and gradient. Hence we now consider a model in which the horizontal cross-section of the coil is effectively concentric annuli of metal and gas that remain constant in size.

4 Linear heat transfer — analytic solutions

In this section we find analytic solutions for linear heat transport within a cylindrical shell. This allows us to consider both radial and axial heat flow simultaneously.

We assume that the coil is a homogeneous region, although with anisotropic heat conductance, so that k_r and k_z are constant. The geometry is illustrated in Figure 8. The solution takes the form of a series whose leading order behaviour is governed by a dominant eigenfunction.

In the linear model, Equation (1) is written in the simpler form

$$\frac{\partial T}{\partial t} = D_r \frac{1}{r}\frac{\partial}{\partial r}\left(r\frac{\partial T}{\partial r}\right) + D_z \frac{\partial}{\partial z}\left(\frac{\partial T}{\partial z}\right). \tag{4}$$

Our boundary and initial conditions are

$$k_z \frac{\partial T}{\partial r} = H(T - T_g), \quad \text{at } r = a, \tag{5}$$

$$k_z \frac{\partial T}{\partial r} = -H(T - T_g), \quad \text{at } r = b, \tag{6}$$

$$T(r, z = 0, t) = T(r, z = L, t) = T_g, \tag{7}$$

$$T(r, z, t = 0) = T_0, \tag{8}$$

where $D_r = k_r/(\rho c_p)$, $D_z = k_z/(\rho c_p)$ are assumed constants, T_g is the external gas temperature, and T_0 the initial temperature of the coil. These equations are scaled using typical values, $t = t_0, r = b, z = L, T = T_g$:

$$t = t_0 t^*, \quad r = b r^*, \quad z = L z^*, \quad u = \frac{T - T_g}{T_0 - T_g}, \tag{9}$$

where r^*, z^*, t^*, u are the nondimensional variables. There is a choice of two obvious time scales t_0, using either D_r or D_z. For the problem of interest it is not clear which is dominant and they are of similar magnitude. Hence, without loss of generality we take

$$t_0 = \frac{L^2}{D_z}.$$

The linearised, nondimensional system is thus

$$\frac{\partial u}{\partial t} = D\frac{1}{r}\frac{\partial}{\partial r}\left(r\frac{\partial u}{\partial r}\right) + \frac{\partial^2 u}{\partial z^2}, \tag{10}$$

$$\frac{\partial u}{\partial r} = +hu, \quad \text{at} \quad r = a, \tag{11}$$

$$\frac{\partial u}{\partial r} = -hu, \quad \text{at} \quad r = 1, \tag{12}$$

$$u(r, z = 0, t) = u(r, z = 1, t) = 0, \tag{13}$$

$$u(r, z, t = 0) = 1, \tag{14}$$

where the * notation has been dropped for convenience, $D = D_r L^2/D_z b^2$ represents the relative diffusivity, $a \in [0,1]$ (strictly a^*) is the ratio of original lengths a/b, and $h = Hb/k_r$. This equation now represents nondimensional cooling of a unit cylinder from initial unit temperature to surrounding temperature zero.

The solution is found by separation and Sturm-Liouville theory. A similar solution for the purely radial case can be found, without derivation, in [2] (page 530). Setting

$$u(r,z,t) = R(r)Z(z)T(t) \tag{15}$$

gives

$$\begin{aligned} Z'' &= \mu Z, \quad Z(0) = Z(1) = 0 && (16)\\ R'' + \frac{1}{r}R' &= \omega R, \quad R'(a) = h\,R(a), \;\; R'(1) = -h\,R(1) && (17)\\ T' &= (D\omega + \mu)T, && (18) \end{aligned}$$

where ω and μ will be the infinite set of eigenvalues. The respective eigenfunction solutions are

$$\begin{aligned} Z &= \sin n\pi\, z, \quad \mu = -(n\pi)^2, \;\; n = 1,2,\ldots && (19)\\ R &= C_0(\lambda r) \equiv J_0(\lambda r) + B\,Y_0(\lambda r), \quad \omega = -\lambda^2, && (20)\\ T &= \exp(-(D\lambda^2 + (n\pi)^2)\,t), && (21) \end{aligned}$$

where B is a constant, and J_0, Y_0 are zeroth order Bessel functions. The boundary conditions at $r = a$ and $r = 1$ give

$$\begin{aligned} -\lambda J_1(\lambda a) - B\lambda Y_1(\lambda a) - hJ_0(\lambda a) - hBY_0(\lambda a) &= 0, && (22)\\ -\lambda J_1(\lambda) - B\lambda Y_1(\lambda) + hJ_0(\lambda) + hBY_0(\lambda) &= 0. && (23) \end{aligned}$$

These have a consistent solution for B when

$$\begin{vmatrix} \lambda J_1(\lambda a) + hJ_0(\lambda a) & \lambda Y_1(\lambda a) + hY_0(\lambda a) \\ -\lambda J_1(\lambda) + hJ_0(\lambda) & -\lambda Y_1(\lambda) + hY_0(\lambda) \end{vmatrix} = 0. \tag{24}$$

This characteristic equation can be solved numerically to find λ, as illustrated in Figure 9 for the case $a = 1/3$ and $h = 1$.

Using equation (15) the full solution is

$$u(r,z,t) = \sum_{n=1}^{\infty} \sum_{m=1}^{\infty} A_{mn}\;\; e^{-(D\lambda_m^2 + (n\pi)^2)t} \;\; \sin n\pi z \;\; C_0(\lambda_m r), \tag{25}$$

where from equation (23)

$$B = - \frac{hJ_0(\lambda) - \lambda J_1(\lambda)}{hY_0(\lambda) - \lambda Y_1(\lambda)}, \tag{26}$$

and A_{mn} are constants found by Sturm Liouville orthogonality as

$$A_{mn} = \frac{\int_0^1 \sin(n\pi z) dz}{\int_0^1 \sin^2(n\pi z)\, dz} \; \frac{\int_a^1 r C_0(\lambda_m r)\, dr}{\int_a^1 r C_0^2(\lambda_m r)\, dr}. \tag{27}$$

These integrals can be evaluated to give

$$A_{mn} = 2\frac{(1-(-1)^n)}{n\pi} \; \frac{\left[\frac{r}{\lambda_m} C_1(\lambda_m r)\right]_a^1}{\left[\frac{r^2}{2}\left(C_0^2(\lambda_m r) + C_1^2(\lambda_m r)\right)\right]_a^1} \tag{28}$$

where C_0, C_1 given by Equation (20). Use has been made of results from [1](chapters 9 and 11) summarised here using $\mathcal{C}_\nu$ and $\mathcal{D}_\nu$ to represent either J_ν or Y_ν:

$$\mathcal{C}_0'(x) = -\mathcal{C}_1(x) \tag{29}$$

$$\int_a^1 r\mathcal{C}_0(\lambda r)\, dr = \left[\frac{r}{\lambda}\mathcal{C}_1(\lambda r)\right]_a^1 \tag{30}$$

$$\int r\, \mathcal{C}_0(\lambda r)\mathcal{D}_0(\lambda r)\, dr = \frac{r^2}{2}(\mathcal{C}_0(\lambda r)\, \mathcal{D}_0(\lambda r) + \mathcal{C}_1(\lambda r)\, \mathcal{D}_1(\lambda r)). \tag{31}$$

The solution given by equation (25) can be evaluated to any degree of accuracy at any point using simple numerical summation. However, the dominant behaviour is given by the leading eigenvalues λ_1 and π. In Figure 9 the eigenvalues are shown as zeros of the characteristic equation (24) with $a = 1/3$ and $h = 1$. Numerically they can be shown to asymptote to being $3\pi/2$ apart.

Figure 10 shows the full solution $u(r, z = 0.5, t = 0.04)$ and the leading eigenfunction, Equation (20) with $\lambda = \lambda_1$, using scaled values $h = 1$, $D = 1$, and $a = 1/3$. This illustrates that the leading eigenfunction dominates the solution and that the position of the cold point, $r = r_c$, can be given by finding the maximum of this eigenfunction. The time dependence is then governed by the time decay of the exponential term $\exp(-(D\lambda_1^2 + \pi^2)t)$.

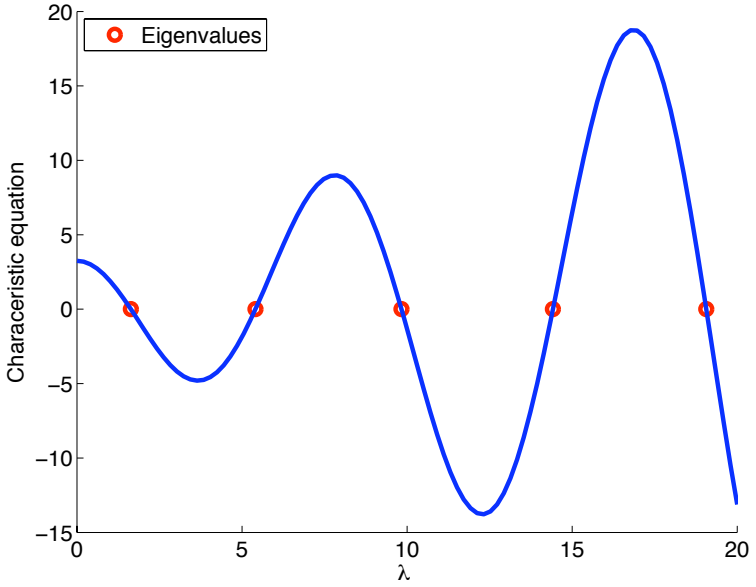

Figure 9: First five eigenvalues shown as zeros of Equation (24) for $h = 1$ and $a = 1/3$.

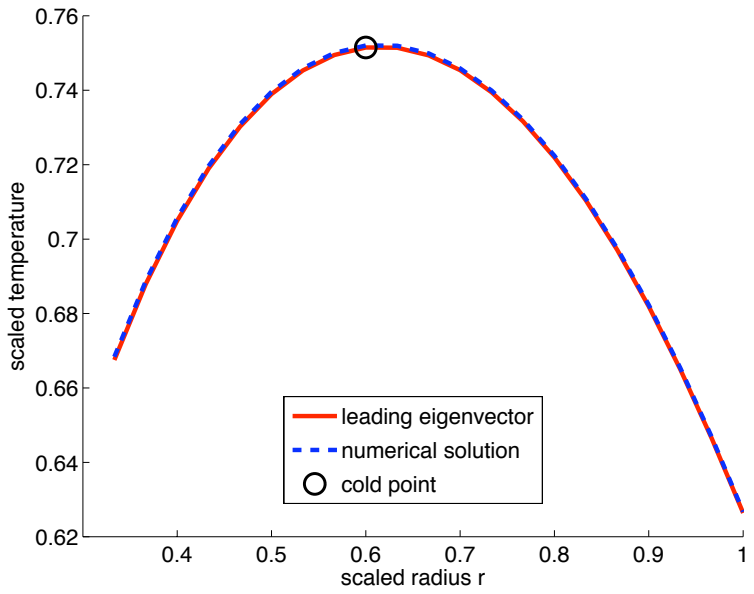

Figure 10: Comparison of full solution $u(r, z = 0.5, t = 0.04)$ and leading eigenfunction (20) for $h = 1$ and $a = 1/3$ with the cold point shown. Hence this eigenfunction is a good predictor of cold point position.

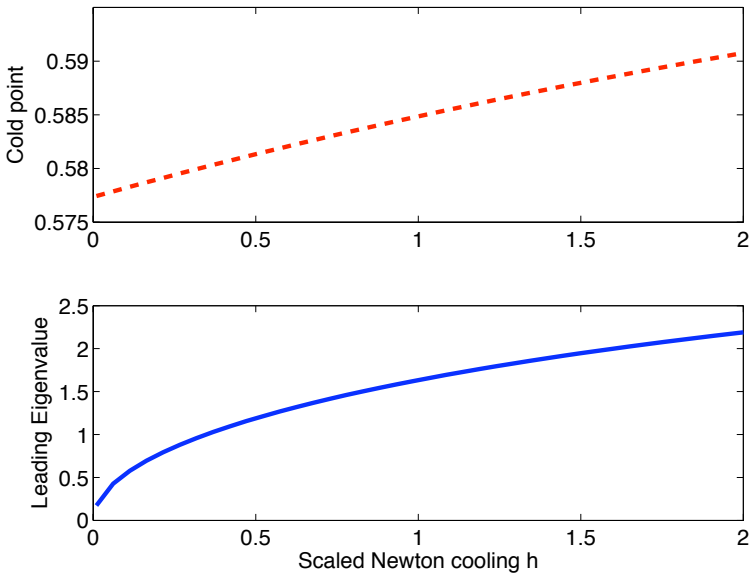

Figure 11: Dependence of the cold point position, $r = r_c$ and leading eigenvalue as functions of scaled surface transfer coefficient h with $a = 1/3$.

Figure 11 shows the dependence of the cold point position and leading eigenvalue as a function of the scaled surface transfer coefficient h with $a = 1/3$, which is comparable to the practical application. Note that the cold point does not vary considerably with h. As h becomes small, the leading eigenvalue becomes small compared with π, the dominant eigenvalue in the z direction; for small h the sides are effectively insulating and diffusion is dominated by the z dependence.

Figure 12 shows a contour plot of the leading eigenvalue as a function of the two parameters governing this variable, h and a. For this application it is unlikely that a will be varied, but this result is included for completeness.

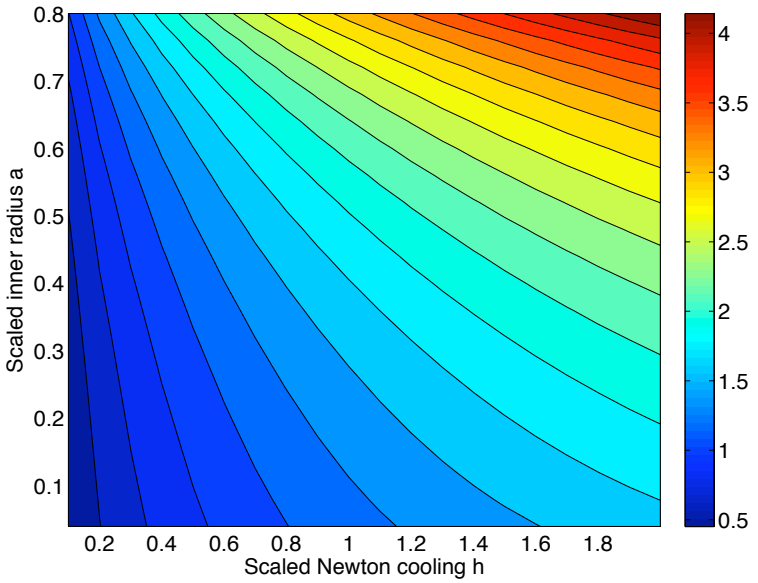

Figure 12: Contour plot showing dependence of the leading eigenvalue as function of scaled surface transfer coefficient h and scaled inner width a.

4.1 Implications for heating times

The key term in the solution (25) is the decay in time factor, which in dimensional terms is

$$e^{-\left(\lambda_1 \frac{D_r}{b^2} + \pi^2 \frac{D_z}{L^2}\right)t} .$$

The first part of the exponent is due to radial heating, the second part is due to axial heating. As noted previously, since the ratio

$$\frac{\lambda_1 D_r L^2}{\pi^2 D_z b^2}$$

is approximately 0.1 (using $\lambda_1 \approx 1$), radial heating is much slower than axial heating. However, the effects as evidenced by the exponential decay term above, are multiplicative - increading the convective transfer term H, for example, by a factor of 5 increases the eigenvalue λ_1 by a factor of 2, which changes the heating time from a scaled value of 1.1 to 1.2, a 10% improvement.

For the cold point to reach the desired soak temperature of 680°C when gas temperature is 710°C and initial temperature is 30°C, the scaled solution u needs to change from the initial value of 1, to the value 30/680. If we ignore radial heating, this happens at the time

$$t = \frac{L^2}{\pi^2 D_z} |\ln(3/68)| \approx 0.32 \frac{L^2}{D_z} \approx 1.28 \frac{\ell^2}{D_z} \ .$$

This formula reduces by 10% if radial heating is included, to give

$$t \approx 1.15 \frac{\ell^2}{D_z} \ .$$

This is almost the same formula as used in Section (3.2), and gives similar heating times.

5 Numerical solutions

In this section we explore numerical solutions to equation (1). For the steel coil application we assume that $k_r = k_r(z)$ so that the radial conductivity across the coil is height dependent. We further consider k_z to be constant, ρ to be constant and c_p to be temperature dependent. Using the same non-dimensionalisation system as with the linear solution we can write the governing equation as

$$\frac{\partial u}{\partial t} = D_r \frac{1}{r} \frac{\partial}{\partial r} \left(r \frac{\partial u}{\partial r} \right) + D_z \frac{\partial^2 u}{\partial z^2} - (u + T_1) \frac{\partial \ln c_p}{\partial t} \tag{32}$$

with boundary and initial conditions the same as equations (11-14) and

$$D_r(z, u) = \frac{c_p(1)}{c_p(u)} \frac{k_r(z)}{k_z} \frac{L^2}{r^2}, \tag{33}$$

$$D_z(u) = \frac{c_p(1)}{c_p(u)}, \tag{34}$$

$$T_1 = \frac{T_g}{T_0 - T_g}. \tag{35}$$

The cumbersome nature of this equation is due to the height dependence $c_p = c_p(u)$. If this is relaxed so that c_p is constant then Equation (10) is recovered exactly.

Using second order, central finite differences, the fully nonlinear version of equation (32) was solved numerically with MATLAB. These experimental results were compared with the analytic solution of Section (4) and found to be accurate for a range of parameter values. Tests for stability and invariance under differing space and time steps were successful.

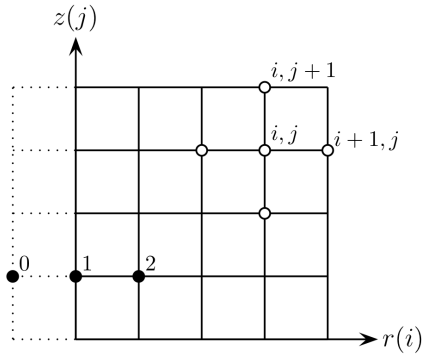

Figure 13: Finite differencing at a central point (i, j) and at a boundary point where a fictitious point is used.

The discretisation used can be illustrated by considering the numerical strategy specifically applied to equation (10), where c_p is assumed constant. If $u(i\,dr, j\,dz, k\,dt) \equiv u^k_{i,j}$ represents the temperature at discretised position and time then

$$u^{k+1}_{i,j} = u^k_{i,j} + dt\left[D\left(\frac{\partial^2 u}{\partial r^2} + \frac{1}{r}\frac{\partial u}{\partial r}\right) + \frac{\partial^2 u}{\partial z^2}\right], \tag{36}$$

$$\frac{\partial^2 u}{\partial z^2} = \frac{u^k_{i,j+1} - 2u^k_{i,j} + u^k_{i,j-1}}{dz^2}, \tag{37}$$

$$\frac{\partial^2 u}{\partial r^2} = \frac{u^k_{i+1,j} - 2u^k_{i,j} + u^k_{i-1,j}}{dr^2}, \tag{38}$$

$$\frac{\partial u}{\partial r} = \frac{u^k_{i+1,j} - u^k_{i-1,j}}{2dr}. \tag{39}$$

The discretisation is shown in Figure 5. The boundaries $z = 0$ and $z = 1$ are easily defined by setting $u = 0$. On the boundaries $r = a$ and $r = 1$ we use a fictitious point outside of the region which is then eliminated by combining the discretisation above with the discretised boundary condition. Hence at

$r = a$ we use the boundary condition, equation (11), and the governing equation (10) and rearrange to find $u^k_{1,j}$:

$$\frac{u^k_{2,j} - u^k_{0,j}}{2dr} = hu^k_{1,j}, \tag{40}$$

$$u^{k+1}_{1,j} = u^k_{1,j} + dt\left[D\left(\frac{\partial^2 u}{\partial r^2} + \frac{1}{r}\frac{\partial u}{\partial r}\right) + \frac{\partial^2 u}{\partial z^2}\right], \tag{41}$$

with the $\frac{\partial^2 u}{\partial r^2}$ and $\frac{\partial u}{\partial r}$ terms involving $u^k_{1,j}$, $u^k_{2,j}$ and the fictitious point $u^k_{0,j}$. Using equation (40) to replace $u^k_{0,j}$ in equation (41) gives the new updated value for $u^{k+1}_{1,j}$. This is similarly applied at $r = 1$.

The numerical solution was found to be sufficiently accurate with a spatial discretisation of 21 points in both r and z directions — although a finer grid size of 41 points was necessary for small values of h. The time step was chosen to minimise computational time while remaining within the stability condition

$$dt < \frac{dx^2}{2D}$$

for all the typical length and diffusion scales in the problem. This numerical solution was also used to find estimates for how many terms are required in the numerical evaluation of the series in Equation (25). As expected, for early times more terms are needed, although 10 terms is usually sufficient for accuracy. At later times, as the exponential term decays more rapidly, less terms are needed.

Figure 14 shows a contour plot of temperature in a cross section of the cylinder, with scaled $h = 0.3$, $t = 0.04$, $a = 1/3$, scaled diffusivity $D = 1/2$ and c_p a constant. These parameter values were chosen to represent realistic values for the coiled steel problem.

Figure 15 shows a cross section of the temperature at $r = 2/3$ with the same parameters as Figure 14. Radial diffusivity is likely to vary with height because of crowning: the uneven thickness across the original cold rolled steel sheets. To investigate this effect, two different solutions are compared, one with the radial diffusivity constant and the other when it varies quadratically as shown on Figure 16. There is very little difference between the solutions. This is because the radial heat transport is so restricted by the surface heat

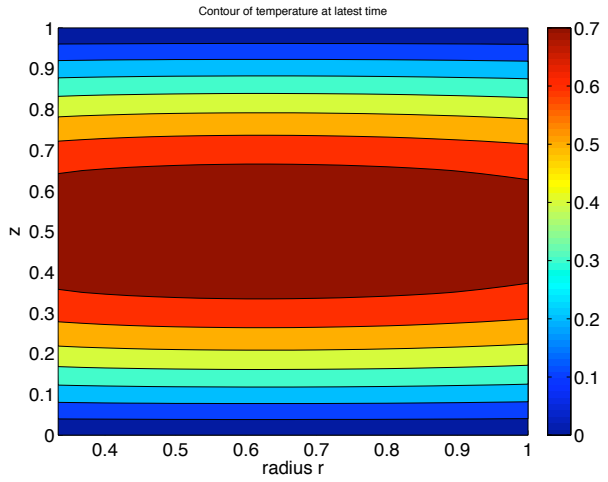

Figure 14: Contour plot of temperature in a cross section of the cylinder, with scaled $h = 0.3$, $t = 0.04$, $a = 1/3$ and scaled diffusivity $D = 1/2$.

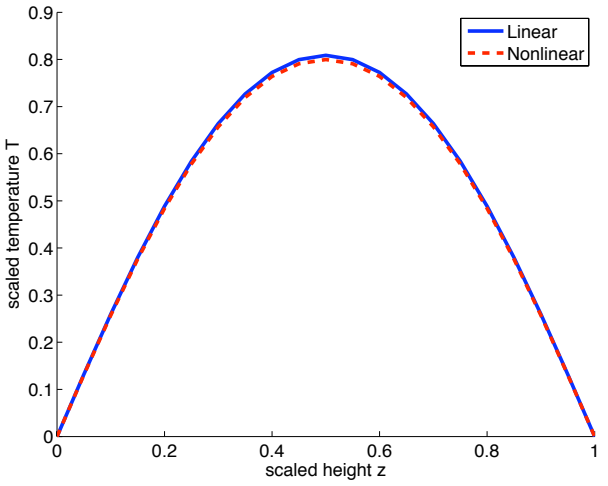

Figure 15: Scaled temperature at $r = 2/3$ versus height with the same parameters as Figure 14. This shows that for Newton cooling on the radial surfaces, varying radial diffusivity has little impact.

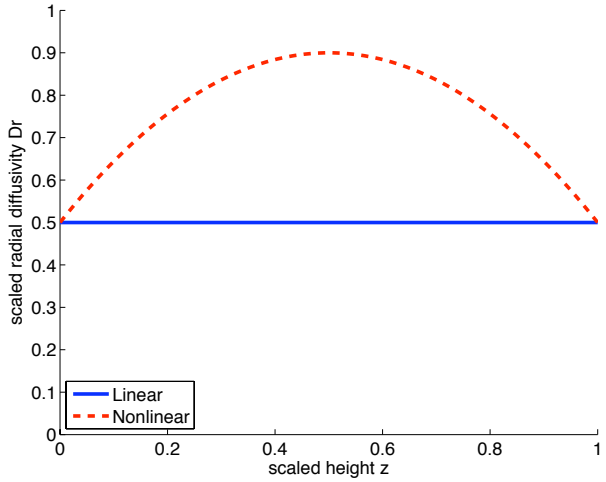

Figure 16: Variation of radial diffusivity with height used in Figure 15 .

transfer coefficient that heat is predominantly diffused vertically. This is also clear from Figure 14.

6 Variable Diffusivity

The diffusivities that have been used in previous sections to estimate heating times have been based on the properties of steel at 1000K. However, steel diffusivity varies with temperature, and is larger at smaller temperatures, so that we have overestimated heating times. The concept of mean action time [3] allows us to calculate by what factor we have overestimated heating time, by considering that the appropriate average diffusivity to take is

$$D_{\text{effective}} = \frac{\int_{T_0}^{T_g} D(T)\, dT}{T_g - T_0} \ . \tag{42}$$

Graphing tabled values of $D(T)$ and fitting a quadratic (using Maple) as illustrated in Figure (17) gives (for T in Kelvin)

$$D \approx 2 \times 10^{-5} - 2.5 \times 10^{-8} T + 4 \times 10^{-12} T^2 \ \ m^2/s \ .$$

and

$$D_{\text{effective}} \approx 1 \times 10^{-5} \ \ m^2/s \ ,$$

which is a factor of three larger than the value of D used at 1000K.

Hence our estimates of heating time are anticipated to be a factor of three too high.

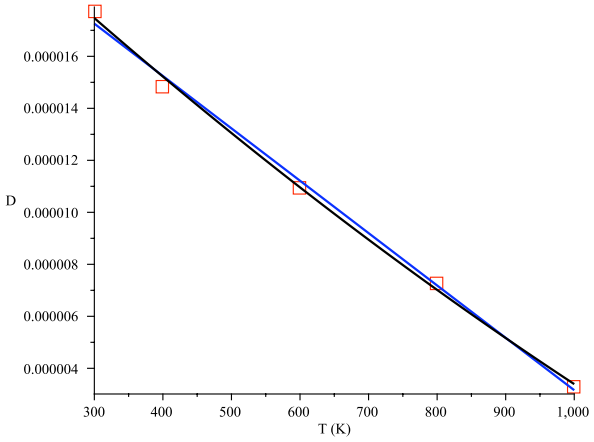

Figure 17: The dependence of diffusivity of steel (m^2/s) on temperature (K), data shown as boxes and a linear and a quadratic fit as curves.

7 Discussion and Conclusions

The analytical and numerical investigations of Sections 4 and 5 suggest that, with the boundary conditions chosen here, the main constriction on the heating of the steel coils is the slow transport of heat through the curved sides of the coils. Further analytical and numerical investigations with radiative heating of all the outer surfaces show a considerable reduction in the heating times.

It is difficult without further experimental data to assess the validity of our assumed boundary conditions. We have ignored the effect of the location of the coil in the furnace but industrial experience suggests that failure of the annealing process is associated with particular grid positions within the

furnace. There will be further radiation within the furnace such as between the sides of the steel coils. Studying the plan of the roof of the furnace further suggests that some parts of the circular top ends of the coils could be partially shielded from the radiation from above, which would break the cylindrical symmetry which we have assumed. Our modelling underscores the importance of radiative heat transport compared with convective transport.

In any case, our results indicate that the primary variable of concern is the vertical lengthscale of the coils, and that considerations such as gauge are secondary, because the radial geometry is in practice independent of gauge, and because radial heat transport is much slower that vertical heat transport. This is because of the boundary conditions rather than the differences in thermal conductivity. Hence, grouping coils by strip width is key to having groups of coils that require the same annealing time in the same batch.

Acknowledgements

We are grateful to the industry representatives Phil Bagshaw, Andrew Mackay and Daniel Yuen for their support and enthusiasm. We also thank the other people who participated in this project who included Seonmin Alm, Barry Cox, Andrew Fowler, Zlatko Jovanoski, Sinuk Kang, Salman Subhani and Ngamta Thamwattana.

References

[1] Abramowitz, M. & Stegun, I. (1970) Handbook of Mathematical Functions, *Dover*, New York.

[2] Budak, B.M., Samarskii, A.A., & Tikhonov, A.N. (1964) *A collection of problems in mathematical physics.* Dover, New York.

[3] Landman, K., & McGuinness, M. (2000) Mean Action Time for Diffusive Processes, *Journal of Applied Mathematics and Decision Sciences*, **4**(2) (2000) pp.125–141.

[4] Sridhar, M.R. &Yovanovicht, M.M. (1994) Review of elastic and plastic contact conductance models: Comparison with experiment. *J. Thermophysics Heat Transfer*, **8**, 633–640.

[5] Stikker, U.O. (1970) Numerical simulation of the coil annealing process, in *Mathematical Models in Metallurgical Process Development*, Iron and Steel Institute, Special Report **123**, 104–113.

[6] Willms, A.R. (1995) An exact solution of Stikker's nonlinear heat equation, *SIAM J. Appl. Math.* **55**, No. 4, 1059–1073.

[7] Xhang, X., Yu, F., Wu, W., & Zuo, Y. (2003) Application of radial effective thermal conductivity for heat transfer model of steel coils in HPH furnace, *Int. J. Thermophysics* **24**, No. 5, 1395–1405.

[8] Zuo, Y., Wu, W., Zhang, X., Lin, L., Xiang, S., Liu, T., Niu, L., & Huang, X. (2001) A study of heat transfer in high-performance hydrogen Bell-type annealing furnaces *Heat Transfer — Asian Research*, **30** (8) 615–623.